https://doi.org/10.22226/2410-3535-2022-4-424-427

True fracture stress of UFG samples of Al 6101 alloy

D. V. Gunderov†,1,2, S. D. Gunderova1,2, D. K. Magomedova3

†dimagun@mail.ru

[1]Ufa State Aviation Technical University, Ufa, 450001, Russia
[2]Institute of Physics of Molecules and Crystals, Ufa Federal Research Center of the RAS, Ufa, 450054, Russia
[3]Saint Petersburg State University, Saint-Petersburg, 198504, Russia

This paper presents the results of studies on the true fracture stresses of the Al alloy 6101 with an ultrafine-grained (UFG) structure processed by equal channel angular pressing — conform (ECAP-C) method and the same alloy after artificial aging (AA state). The grain size in the UFG state was about 500 nm. Aging particles and Al_3Fe particles were present in the structure of AA and UFG state. Strength and yield stress increase as a result of the formation of UFG structure. The true strain to failure in AA and UFG states of 6101 alloy, taking into account the measurement error, is the same. In this case, the true fracture stress of samples with the UFG structure is markedly higher than the true fracture stress of samples with the AA structure. An explanation for the increase in the true fracture stress of specimens with UFG structure based on a generalization of the Hall-Petch relation and the Zener-Strauss model, a criterion of pore formation on the particle, is proposed.

Keywords: bulk nanomaterials, equal-channel angular pressing — conform (ECAP-C), dislocations, true stresses, fracture stresses, true fracture stresses.

1. Introduction

It is well known [1,2] that the dependence of the yield stress σ_y and flow stress $\sigma(\varepsilon)$ of polycrystalline metallic materials on the grain size is determined by the Hall-Petch equations [1,2]

$$\sigma_y = \sigma_{0y} + k_y d^{-1/2}, \quad (1)$$

$$\sigma(\varepsilon) = \sigma_0(\varepsilon) + k(\varepsilon) d^{-1/2}, \quad (2)$$

where σ_{0y}, k_y are material constants, and $\sigma_0(\varepsilon)$ and $k(\varepsilon)$ are constant parameters for a given value of strain. The parameter σ_{0y} is the "friction stress" of the movement of dislocations in crystal lattice, the parameter k_y determines the grain boundary strengthening.

The yield stress and flow stress of polycrystals depend not only on the average grain size, but also on many other parameters of the grain structure, such as, for example, grain size distribution [3], texture [4], grain boundary (GB) structure, etc. However, this does not violate the validity of relations (1) and (2), but leads to a change in k_y and $k(\varepsilon)$, as well as the exponent x in the relation $\sigma_y = \sigma_0 + k_y d^x$. Several models have been proposed to explain the Hall-Petch (HP) relationship (1). The model of dislocation pile-ups is one of the most common of these [1,2,6,7].

In the last three decades, a new approach to improve the properties of metallic materials due to the formation of ultrafine-grained (UFG) and nanostructured states in them using severe plastic deformation (SPD) methods has attracted a great interest [10–12]. The formation of UFG structures in metals and alloys by means of grain refinement to a size of less than 1 μm can significantly improve their strength characteristics. A large number of papers [13–17] are devoted to the relationship between the parameters of grain structure and the mechanical properties of materials obtained by SPD and the deformation features in them. In particular, the violation of the Hall-Petch relationship for grain sizes in the nanozise-range (20–50 nm) is found, where a decrease in the yield stress is observed with a further decrease in grain size [13–15]. On the other hand, in some cases, UFG materials with a grain size of 100–1000 nm can exhibit higher strength properties than the ones predicted by the Hall-Petch relationship, which is associated with the state of grain boundaries and segregations at the boundaries [18–20]. However, the main attention in most works on the mechanical behavior of UFG materials has been paid to such parameters as the yield strength, tensile strength, and ductility. Various aspects of fatigue failure of the UFG materials have been studied [10,11]. Though we note that one can also obtain such a parameter as the true fracture stress from tensile tests [21], which is also of scientific interest. Previously, it was shown in [21,22] that the true fracture stress σ_{Ifrac} of UFG titanium, TiNi alloy in the UFG state, exceeds σ_{Ifrac} of these materials in conventional coarse-grained state. Nevertheless, the analysis and explanation of this was not given in [21,22].

Al 6101 alloy has a high electrical conductivity and strength level, which allows it to be widely used for overhead power lines. The alloy exhibits a tensile strength of about 250 MPa after conventional thermal treatment (quenching with ageing) [23,24]. An additional increase in strength (and retention of electrical conductivity) in conductive aluminum materials can be achieved by forming the UFG structure using SPD [25–28]. There are quite a few works devoted to the study of the properties of aluminum alloys, and specifically 6101 alloy, which showed an increase in the strength after SPD, including after equal-channel angular pressing according to the "Conform" scheme (ECAP-C) [25,26]. In [29,30], studies on the features of the mechanical behavior, fracture and pore formation before the tensile failure of UFG Al 6101 samples were carried out. It is shown that Al_3Fe intermetallic particles based on impurity iron play an important role in fracture. These particles with a size of several microns are the centers

for the nucleation of discontinuities in the form of nanopores and the subsequent fracture of the 6101 alloy samples [29,30]. However, it is important to study the features of the mechanical behavior of UFG Al 6101 alloys, in particular, the construction of true strain-stress curves in static tension, and further analysis of the causes of the increased true fracture stress, which is the subject of this work.

2. Samples and research methods

The commercial heat-strengthened aluminum 6101 alloy, which belongs to the Al-Mg-Si system, was chosen as the research material; its chemical composition is given in Table 1.

The initial billets of 6101 alloy were in the form of rods (wire rod) with a diameter of 11 mm. The alloy was subjected to thermal treatment according to the following mode: quenching (heating up to 550°C) + artificial aging at 170°C for 12 hours ("AA" state). Hardening in the AA state is mainly due to the precipitation of β'(Mg_2Si) or β''+β'-phases with a particle size of about 0.03 μm.

The ECAP-C processing to obtain the UFG state was carried out considering the experience of [27]. Rods with an initial diameter of 10 mm were subjected to the ECAP-C treatment according to the following mode: preheating at 550°C for 2 hours, quenching in water, and 4 cycles of the ECAP-C processing were immediately carried out at room temperature through the Bc route, the channel conjugation angle was 130°. Thus, the alloy was subjected to ECAP-C in the freshly quenched state of the solid solution. The solid solution decomposition and natural aging took place within several days after completion of the ECAP-C process in the material in the UFG state, which additionally increased the alloy strength.

Mechanical tests on static tension with a fixed tensile rate of 1.4×10^{-4} s^{-1} were carried out on a Shimadzu machine at room temperature. The change in the length of the samples was recorded using a video extensometer. Cylindrical specimens with geometric dimensions of the gage length $l=5$ mm, gage diameter $d=5$ mm were used for mechanical tests [29]. Three samples for each condition were tested.

The engineering tensile stress-strain diagrams and parameters derived from them incorrectly reflect the behavior of the material itself. The true strain - true stress diagram correctly describes the mechanical behavior of the material.

The engineering strain:

$$\varepsilon = \Delta l / l_0, \tag{3}$$

Here, l_0 is the original length of samples, Δl is the increase in length, $\Delta l = l - l_0$. The true strain is equal to

$$e = \ln\left(S_0 / S_t\right) = \ln\left(l+l\right) / l_0, \tag{4}$$

where S_t is the current area of section of the sample.

True deformation curves for the materials are plotted in the "true stresses σ_i - true strains e" coordinates (using the technique from [12,13]).

The calculation of σ_i and e values was carried out according to the formulas — up to the moment of deformation localization (from the constancy of volumes):

$$\sigma_i = \sigma \, S / S_0 = \sigma \cdot d^2 / d_0^2 = \sigma \cdot l / l_0, \tag{5}$$

where σ is the engineering stress,

$$e_i = e_1 = \ln(l / l_0). \tag{6}$$

However, expression (5) and (6) are valid only up to the moment of deformation localization. After the neck formation, we determine the end point of the curve. The cross-sectional area of the neck of the sample S_p is measured after the fracture. True fracture strain e_{frac}:

$$e_{frac} = \ln\left(S_0 / S_{frac}\right), \tag{7}$$

where S_0 is the initial area of the sample, S_{frac} is the fracture area of the sample after the failure.

The true fracture stress σ_{Ifrac} is found by the formula:

$$\sigma_{Ifrac} = \sigma_{frac} \cdot S_0 / S_{frac}, \tag{8}$$

where σ_{frac} is the fracture stress according to the engineering tensile diagram. In the first approximation, we can assume that in the section from σ_i (the beginning of deformation localization) to fracture, the true stress on the samples increases linearly with the growth of true strain. We plot the σ_{Ifrac} point at e_{Ifrac} on the true strain-true stress curve. We construct the curve in the area of deformation localization in the first approximation by connecting $\sigma_{iв}$ and σ_{Ifrac}.

As a result, we obtain the required true strain-true stress diagram.

3. Results

Previous studies have shown that the grain size is more than 100 μm in the coarse-grained state after AA [29]. There are 2 types of intermetallics in the AA structure: age-hardening particles Mg_2Si with a size of about 20 nm and Al_3Fe inclusions with a size of about 10 μm [29]. Al_3Fe inclusions were formed due to the presence of impurity iron at the stage of alloy casting, and these inclusions do not dissolve and do not transform during the thermal treatment used. In the UFG state, the grain size is about 500 nm, and there are also aging particles (formed as a result of natural aging) and Al_3Fe intermetallics [29].

The engineering tensile diagrams for the UFG and AA states are shown in Fig. 1a.

The true tensile diagrams of the AA and UFG states were constructed using the method described above based on the obtained engineering tensile diagrams, considering the area of the samples after fracture, which is determined from the SEM images (Fig. 1b).

Table 2 shows the mechanical properties determined from the curves for the AA and UFG structures.

Tests have shown that samples in the UFG state have strength and yield stress 25% higher than in the AA state.

Table 1. Chemical composition of the Al 6101 alloy (wt.%).

Alloy grade	Limit	Al	Si	Fe	Cu	Mg	Zn	B	Ti+V+Cr+Mn
6101	Max	base	0.60	0.30	0.01	0.60	0.02	0.01	0.015

Previously, an approximately similar increase in the strength of the 6101 alloy as a result of ECAP-C was shown in [25, 26], where tests were carried out on cylindrical specimens according to All-Union State Standard (GOST). It can also be seen that the true strain to fracture of the 6101 alloy in the AA and UFG state, considering the measurement error, is the same. In this case, the true fracture stress of the UFG samples is noticeably higher than that of the AA samples. As already mentioned, the increase in strength and yield stress as a result of ECAP-C is determined by a decrease in the grain size of an alloy according to the Hall-Petch relationship, whereby the more stress is required for the flow of dislocations with a decrease in the grain size. However, the question of why the true fracture stress of the samples increases during the UFG structure formation requires special discussion.

In the 6101 alloy, the pore formation and subsequent fracture during deformation occurs on Al_3Fe inclusions [29, 30, 31]. The well-known Zener-Stroh model [32] is the pore formation criterion, which states that a pore on a particle is formed when the stress σ reaches a certain critical value σ_r:

$$\sigma > \sigma_r \qquad (9)$$

On the other hand, the Hall-Petch relationship [1] has the following explanation (Fig. 2): according to the model of dislocation pile-ups, slip in a polycrystal is transferred from grain to grain through the grain boundary when the stress concentration near the head of the cluster of dislocations formed near the boundary exceeds some critical value τ_c. The number of dislocations in a cluster with length L at an active uniform shear stress τ is equal to $n = \alpha_1 \pi L\tau / Gb_L$, where α_1 is the coefficient close to unity, depending on the nature of the dislocations, G is the shear modulus, b_L is the Burgers vector of a dislocation [9]. The stress acting on the head dislocation is equal to $\tau_1 = n\tau$ [9], therefore $\tau_1 = \alpha_1 \pi L\tau^2 / Gb_L$. Assuming that the friction force τ_0 acts on the dislocations in the slip plane and the length of the pile-ups is equal to half the grain size d, we obtain the equation for the shear stress that ensures the flow of dislocations through the grain boundary:

$$\tau = \tau_0 + \left(\frac{2Gb_L \tau_c}{\alpha_1 \pi} \right)^{1/2} d^{-1/2}, \qquad (10)$$

where τ_c is the critical value of τ_1, at which the head dislocation crosses the boundary. The flow of dislocations through the grain boundary determines the yield stress as a macroplastic deformation of a polycrystalline material (in contrast to microplastic deformation, where the flow of dislocations is within the individual grains favorably oriented for deformation).

In other words, the number of dislocations n accumulating at the grain boundary during microstrain (flow within one grain) increases with the grain size d, which causes an increase in stress τ at the boundary. The movement of dislocations into a neighboring grain occurs at a certain critical stress $\tau_c = \tau_1 + \tau$ where τ is the external stress on the sample.

A similar model can be developed — extended to the fracture stress (Fig. 3). The number of dislocations n_p accumulating at the grain/particle interface increases with an increase in the path length/generation of dislocations in accordance with the growth of the grain size. And at the grain/particle interface, dislocation pile-ups n_p cause stresses σ_{pp}. To achieve the critical stress σ_r, which causes a rapture at the material/particle interface, and to form a pore, one can use the equation from the model of dislocation pile-ups:

$$\sigma_r = \sigma_c - \sigma_{pp} \qquad (11)$$

where $\sigma_{pp} = (2Gb_L\sigma_c / \alpha\pi)^{1/2} d^{1/2}$.

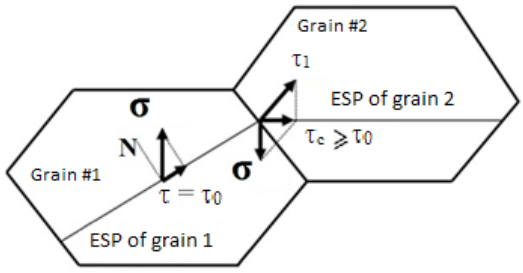

Fig. 2. Scheme illustrating the relay transfer of plastic deformation in a polycrystal, which determines the Hall-Petch relationship. EPS — easy slip plane.

Table 2. Mechanical characteristics of the 6101 alloy in the AA and UFG states. δ_{hom} (%) is the homogenous deformation, e_{frac} — true fracture strain, $\sigma_{I\,frac}$ — true fracture stress, the error of stress was about ±15 MPa, error of δ was about ±3%, $e_{frac} \pm 0.3$.

Structure state	YS, MPa	UTS, MPa	δ_{hom}, %	d, %	σ_{Ifrac}, MPa	e_{frac}
AA	230	265	12	42	365	0.92
UFG	305	350	5	48	565	0.95

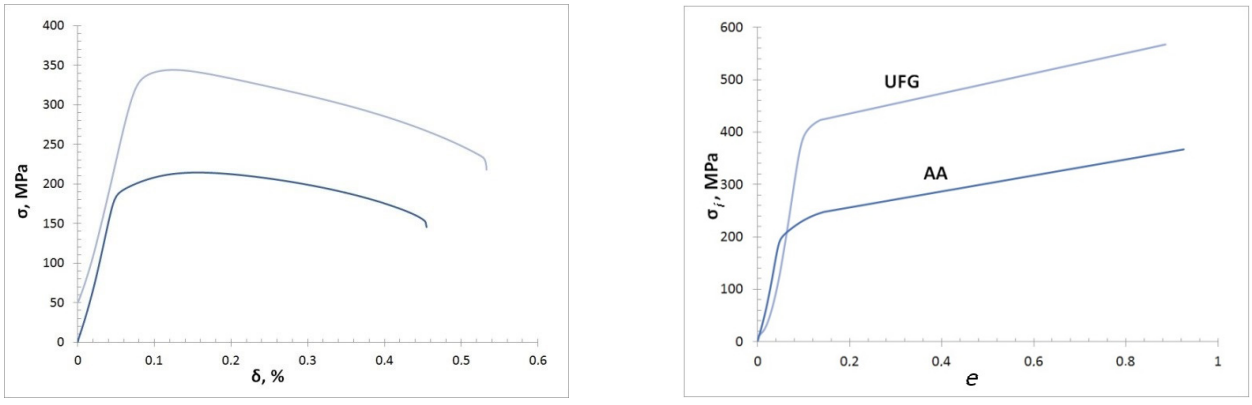

a b

Fig. 1. Diagrams for: artificial aging (AA) and ultrafine-grained (UFG) state of 6101 alloy under engineering stress-strain (a) and true stress-strain (b). σ_i — true stresses (the most typical curves are shown).

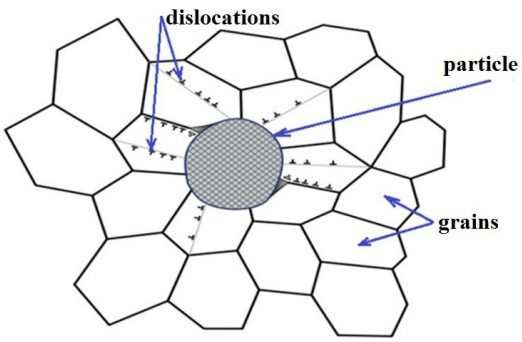

Fig. 3. Diagram explaining the increased true fracture stress in materials with a smaller grain size.

In turn, fracture occurs due to the formation and coalescence of pores arising during the pore deformation, and hence σ_r determines σ_{Ifrac}.

$$\sigma_r \approx \sigma_{Ifrac} \quad (12)$$

Thus, the joint analysis and compilation of the conditions of the dislocation cluster pile-ups model and the Zener-Stroh model explains the increased true fracture stress in UFG materials.

4. Conclusions

The ECAP-C treatment of the 6101 alloy results in a 25% increase in strength and yield stress over conventional quenching and aging treatment, referred to as artificial aging.

The true stress-strain diagrams of the 6101 alloy samples in the AA and UFG states are plotted, from which it follows that the true strain to fracture of the 6101 alloy in both states, considering the measurement error, is the same. In this case, the true fracture stress of the UFG samples is noticeably higher than that of the AA samples.

The increase in the yield stress and the associated tensile strength in the UFG state is explained by the Hall-Petch relationship: a greater external stress is required to set the flow of dislocations as the grain size decreases.

An explanation is proposed for the increase in true fracture stress of samples during grain refinement based on the compilation of the Hall-Petch relationship and the Zener-Stroh model — the criterion for pore formation on a particle when stresses at the matrix/particle boundary reach critical values.

Acknowledgments. The research was supported by the Russian Science Foundation project 22-19-00347 and the Megagrant project No. 075-15-2022-1114. We express our gratitude to Prof. A. A. Nazarov for fruitful discussion of the work.

References

1. E. O. Hall. Proc. Phys. Soc. 64 (1), 747 (1951). Crossref
2. N. J. Petch. J. Iron and Steel Inst. 174, 25 (1953).
3. J. J. Bucki, K. J. Kurzydlowski. Mater. Charact. 29, 375 (1992). Crossref
4. N. Hansen, D. J. Jensen. Strength of Metals and Alloys. Vol. II. London, Freund (1991) 953 p.
5. J. W. Wyrzykowski, M. W. Grabski. Philos. Mag. A. 53 (4), 505 (1986). Crossref
6. J. C. M. Li, Y. F. Chou. Metall. Trans. 1, 1145 (1970). Crossref
7. A. H. Cottrell. The Mechanical Properties of Matter. New York, Wile (1964) 430 p.
8. U. F. Kocks. Metall. Trans. 1, 1121 (1970). Crossref
9. J. D. Eshelby, F. C. Frank, F. R. N. Nabarro. Philos. Mag. 42 (327), 351 (1951). Crossref
10. A. P. Zhilyaev, T. G. Langdon. Prog. Mater. Sci. 53, 893 (2008). Crossref
11. R. Z. Valiev, A. P. Zhilyaev, T. G. Langdon. Bulk Nanostructured Materials. Hoboken, NJ, John Wiley & Sons, Inc (2013). Crossref
12. R. Z. Valiev, Y. Estrin, Z. Horita, T. G. Langdon, M. J. Zehetbauer, Y. T. Zhu. JOM. 58, 33 (2006). Crossref
13. C. S. Panda, K. P. Cooper. Prog. Mat. Sci. 54 (6), 689 (2009). Crossref
14. M. Yu. Gutkin, I. A. Ovid'ko, C. S. Pande. Philos. Mag. 84 (9), 847 (2004). Crossref
15. A. A. Nazarov. Philos. Mag. A. 69 (2), 327 (1994). Crossref
16. A. A. Nazarov, A. E. Romanov, R. Z. Valiev, B. Baudelet. Strength of Materials. Japan, JIMIS (1994) pp. 877–879.
17. A. A. Nazarov. Scripta Mater. 34 (5), 697 (1996). Crossref
18. R. Z. Valiev, N. A. Enikeev, M. Y. Murashkin, V. U. Kazykhanov, X. Sauvage. Scr. Mater. 63 (9), 949 (2010). Crossref
19. M. M. Abramova, N. Enikeev, R. Z. Valiev. Mater. Lett. 136, 349 (2014). Crossref
20. J. G. Kim, N. A. Enikeev, J. B. Seol, M. M. Abramova, M. V. Karavaeva, R. Z. Valiev, C. G. Park, H. S. Kim. Scientific Reports. 8, 11200 (2018). Crossref
21. D. V. Gunderov, A. V. Polyakov, A. A. Churakova, I. P. Semenova, G. I. Raab, R. Z. Valiev, E. Emaletdinova, I. Sabirov, J. Segurado, V. D. Sitdikov, I. V. Alexandrov, N. A. Enikeev, R. Z. Valiev. Materials Science & Engineering A. 562, 128 (2013). Crossref
22. D. V. Gunderov, G. Maksutova, A. Churakova, A. Lukyanov, A. Kreitcberg, G. I. Raab, I. Sabirov, S. Prokoshkin. Scripta. 102, 99 (2015). Crossref
23. K. Sedat. Mater. Design. 27, 821 (2006). Crossref
24. G. Lin, Z. Zhang, H. Wang, K. Zhou, Y. Wie. Mater. Sci. Eng. A. 650, 210 (2016). Crossref
25. I. Sabirov, M. Murashkin, R. Z. Valiev. Mater. Sci. Eng. A. 560, 1 (2013). Crossref
26. M. Yu. Murashkin, I. Sabirov, X. Sauvage, R. Z. Valiev. J. Mater. Sci. 51, 33 (2016). Crossref
27. M. Murashkin, A. Medvedev, V. Kazykhanov, A. Krokhin, G. Raab, N. Enikeev, R. Z. Valiev. Metals. 5, 2148 (2015). Crossref
28. X. Sauvage, E. V. Bobruk, M. Y. Murashkin, Y. Nasedkina, N. A. Enikeev, R. Z. Valiev. Acta Mater. 98, 355 (2015). Crossref
29. D. K. Magomedova, M. A. Efimov, A. A. Churakova, D. V. Ryabokon, D. V. Gunderov. Journal of Physics: Conf. Ser. 1474, 012027 (2020). Crossref
30. D. K. Magomedova, A. A. Churakova, D. V. Gunderov. Journal of Physics: Conf. Ser. 2231, 012018 (2022). Crossref
31. M. E. Drits, A. M. Korolkov, Yu. P. Guk, L. P. Gerasimova, E. N. Petrova. Destruction of aluminum alloys under tensile stresses. Moskva, Nauka (1973) 215 p. (in Russian)
32. C. A. Zener. Phys. Rev. 69, 128 (1946). Crossref